RSC Advances

PAPER

View Article Online
View Journal | View Issue

Cite this: *RSC Adv.*, 2021, **11**, 35245

Dual-purpose high-efficiency air filter paper loaded with reactive zirconium hydroxide for the filtration aerosols and degradation of chemical warfare agents†

Xingqi Huang,[a] Ting Zhao,[b] Hongpeng Zhang,[a] Chunxiao Yan, *[a] Jiulong Sha,[c] Huamin Tang,[a] Haiyan Zhu[a] and Yue Wu[b]

Traditional air filter papers can only filter toxic aerosols without the function of decontamination. If the poison stagnating in the paper is desorbed, it may pose a secondary threat to personnel and make it more difficult to dispose of the scrapped paper. Using an alkali-free glass fiber as the base material and zirconium hydroxide as the decontaminant, a self-decontaminating air filter paper that can degrade HD and VX simultaneously was successfully prepared by an intra-pulp addition method, with high filtration efficiency, low pressure drop and moderate tensile strength. The physicochemical properties were characterized by FE-SEM, EDX, XRD and TGA, and the results indicated that $Zr(OH)_4$ was dispersed uniformly in the paper and filled in the interstices of the glass fiber. The preparation of the composite material had no impact on the structure of fibers and $Zr(OH)_4$. The preparation technology of the self-decontaminating air filter paper was optimized. It was found that the paper with a fiber grammage of 50 g m^{-2}, the adhesive of 2% and a $Zr(OH)_4$ retention rate of 175.0 wt% could completely degrade HD and VX, whose conversion rate exceeded 99.0%, and had a tensile strength of 0.1193 kN m^{-1}, a filtration efficiency of 99.995%, and a pressure drop of 313.6 Pa. Using GC-MS to detect the decontamination products, it was speculated that HD mainly underwent hydrolysis and elimination reactions, VX mainly underwent hydrolysis and polymerization reactions, and their products were non-toxic or low-toxic. The reaction kinetics of HD and VX on the paper was investigated and the half-lives were 2.6 h and 16.2 min, respectively, which demonstrated an outstanding degradation performance. This work manifested for the first time that the air filter paper can be optimized as an efficient self-decontaminating material, which will open up new possibilities for the design and manufacture of multifunctional protective materials.

Received 15th September 2021
Accepted 14th October 2021

DOI: 10.1039/d1ra06903a

rsc.li/rsc-advances

1. Introduction

Since the chlorine attack in the Battle of Ypres during World War I, chemical weapons began to be used on a large scale on the battlefield,[1,2] and protective equipment against chemical weapons came into existence. Traditional protective materials are generally based on the adsorption and catalysis of toxic vapors, filtration of toxic aerosols, and resistance to the penetration of toxic droplets, rather than degrading them. As a result, the toxic chemicals may be desorbed from protective equipment used in poisonous areas.[3,4] It not only poses a threat to personnel and equipment, but also makes it more difficult to dispose of scrap. In recent years, the integrated technology for protection and decontamination has continued to develop, and a number of protective materials, such as carbon[5] and polymer materials,[6–8] with self-decontamination function have been exploited one after another. For example, John Walker *et al.*[9] added organic phosphate dehydratase OPAA and modified dehydratase OPAA-C18 coated with high-branched

[a]*Department of Chemistry Defense, Institute of NBC Defense, Beijing 102205, China. E-mail: yanchunxiao1964@sina.cn*

[b]*Shanxi Xinhua Chemical Defense Equipment Research Institute Co., Ltd, Taiyuan 030000, China*

[c]*Guangxi Key Laboratory of Clean Pulp & Papermaking and Pollution Control, School of Light Industry and Food Engineering, Guangxi University, Nanning 530004, China*

† Electronic supplementary information (ESI) available: (a) FE-SEM image and EDS spectral result of all the elements of SD-AFP; (b) EDS diagram (Fig. S1), tensile strength of SD-AFP: (a) tensile strength varies with fiber grammage; (b) tensile strength varies with the amount of adhesive (Fig. S2), linear parameters of the tensile strength change varies with the fiber grammage (Table S1), linear parameters of the tensile strength change varies with the amount of adhesive (Table S2), filtration efficiency of SD-AFP: (a) filtration efficiency varies with the amount of adhesive; (b) filtration efficiency varies with the fiber grammage (Fig. S3), pressure drop of SD-AFP: (a) pressure drop varies with the amount of adhesive; (b) pressure drop varies with the fiber grammage (Fig. S4), linear parameters of the pressure drop change varies with the amount of adhesive (Table S3), linear parameters of the pressure drop change varies with the fiber grammage (Table S4), linear parameters of the pressure drop change varies with the retention rate of ZH (Table S5). See DOI: 10.1039/d1ra06903a

polyvinyloxazoline into the spinning dope and adopted a high-voltage electrostatic fiber-forming process to obtain a self-detoxifying membrane, which can effectively promote the hydrolysis of the chemical warfare agents (CWAs) simulant diisopropylfluorophosphate (DIFP). Furthermore, lithium alkoxide was inserted into a zirconium metal–organic framework (MOF) and deposited on the textile to form a composite fabric protective material with self-decontaminating function, which has achieved great hydrolysis performance against P–F, P═O and C–Cl bonds.[3] Researchers in the relevant field use methods such as electrospinning, dipping, spraying, and atomic layer deposition (ALD) coating to add metal oxides and MOF materials[10,11] to functional filter media or protective clothing, which can be used to degrade CWAs.[12] However, research previously conducted on integrated materials for protection and decontamination mainly focused on skin protection materials. There is no public report on the research of air filter paper (AFP) used for decomposing toxic aerosols.

Sulfur mustard (2,2′-dichloroethyl sulfide), also known as HD, is called "the king of CWAs". It is a blister agent with high toxicity, targeting the human skin and mucous membranes. It can cause tissue cell necrosis and ulceration, and there is no specific drug to cure it.[13,14] The nerve agent *O*-ethyl *S*-(2-diisopropylamino)ethyl methylphosphonothiolate, better known as VX, poses a severe contact risk, as it is readily absorbed through the skin. After being poisoned, it can destroy the normal conduction function of the nervous system in a short time, causing symptoms such as difficulty in breathing, severe convulsions and loss of consciousness.[15] Worst of all, a few milligrams can cause fatal injury,[16] just as happened with Kim Jong Nam. High-efficient AFP does not have the function of degrading CWAs such as VX and HD, which brings certain hidden hazards to the use of gas masks and the handling after tasks. It is of great significance to study the modification of AFP to endow it with the function of self-decontamination.

Zirconium hydroxide (ZH) is an amorphous porous reagent with both acid–base and redox properties, which is benefited from multifarious active centers, for instance, coordinated unsaturated metal cations ($Zr^{\delta+}$), oxygen vacancies, bridging hydroxyl groups (b-OH) showing Brønsted acidity, and terminal hydroxyl groups (t-OH) showing Brønsted basicity.[17,18] Excellent adsorption performance is obtained due to its porous structure, which can be combined with activated carbon as an adsorbent to adsorb persistent anionic reactive dyes[19] and water pollutants.[20–22] Variable-temperature *in situ* attenuated total reflection (ATR) infrared spectroscopy was employed to study the reaction kinetics of dimethyl methylphosphonate (DMMP) by ZH in the $\rho(PCH_3)$ mode. It was found that both adsorption and decomposition processes of DMMP occurred and the pseudo-second-order model best fitted the reaction data.[23] Moreover, American scholars evaluated the degradation ability of ZH on HD and VX. The half-lives monitored by NMR were 2.3 h and 1.0 min respectively, and the phosphate product was detected at the same time.[24] Subsequently, extensive research was carried out on self-decontaminating materials composited with ZH. Jeon *et al.*[25] used an electrochemical synthesis method to prepare nanoscale ZH films on metal substrates, which can rapidly decompose DMMP, a nerve-agent simulant. ZH/PVB nanofibrous membranes were prepared by an electrospinning method to degrade DMMP, with a half-life of 4 min.[26] Electrospinning nylon-6,6 fabric as a substrate, ZH obtained by hydrolyzing $Zr(OBu)_4$ was coated onto its surface *via* a sol–gel reaction to obtain a self-detoxifying membrane for nerve agents.[27] Electrospinning and solution-spinning were used to synthesize fibers for compositing with decontaminants to degrade CWAs. However, AFP was made of glass fiber, whose raw materials are mainly SiO_2 and easy to obtain. Glass fiber is formed by high-temperature melting into filaments, which can be produced commercially. Making paper on this basis will make it easier to produce industrially. Different from skin protection materials, the AFP has pore structures composed of numerous interlaced fibers, with low strength and burst resistance. It is toilless to damage the structure when it is modified. Hence, it is of great importance to find a mild decontaminant and a suitable modification method. Intra-pulp addition is a method of adding chemicals to the pulp during beating or in the pulp supply system to enable the paper to obtain antibacterial, flame-retardant, deodorizing and other functions.[28,29] Not only is the process simple to operate, but the additives are also evenly distributed in the paper for good modification effect. This method is generally suitable for water-insoluble inorganic materials in powder form such as ZH. The problem that additives are easy to lose during the paper-making process can be solved by adding fixatives.[30] Taking into account that ZH will not damage the composition and structure of the paper and has a good degradation effect on HD and VX, it was added to the AFP to give it the function of decontamination.

The purpose of this paper is to explore and develop a methodology for producing self-decontaminating air filter paper (SD-AFP), which can maintain high filtration efficiency, low pressure drop and moderate tensile strength of AFP as well as degrade HD and VX simultaneously. Specifically, it is designed to add ZH to the pulp during the paper-making process and alter the three key parameters, namely, filtration efficiency, tensile strength and pressure drop by regulating the grammage of the fiber, the amount of adhesive and the retention of ZH. In fact, it is important to solve the problem of the dispersion and control the retention rate of zirconium hydroxide in the paper during the paper-making process. Meanwhile, there is certain difficulty to control the amount of adhesive to enhance the tensile strength as well as make it distributed uniformly. By performing FE-SEM, XRD and TGA to characterize the structural properties of the obtained SD-AFP, the degradation performance to HD and VX was investigated, and the kinetic processes and product characteristics were further analyzed.

2. Experimental section

2.1 Materials

Petroleum ether, acetonitrile, absolute ethanol, sodium tetraborate (borax), anhydrous sodium sulphate (AR grade, Beijing Reagent Factory), dichloromethane (HPLC grade, Puredil), tributyl phosphate (98%, Alfa Aesar) and derivatization reagent (Aladdin), consisting of 99% *N*,*O*-bis(trimethylsilyl)

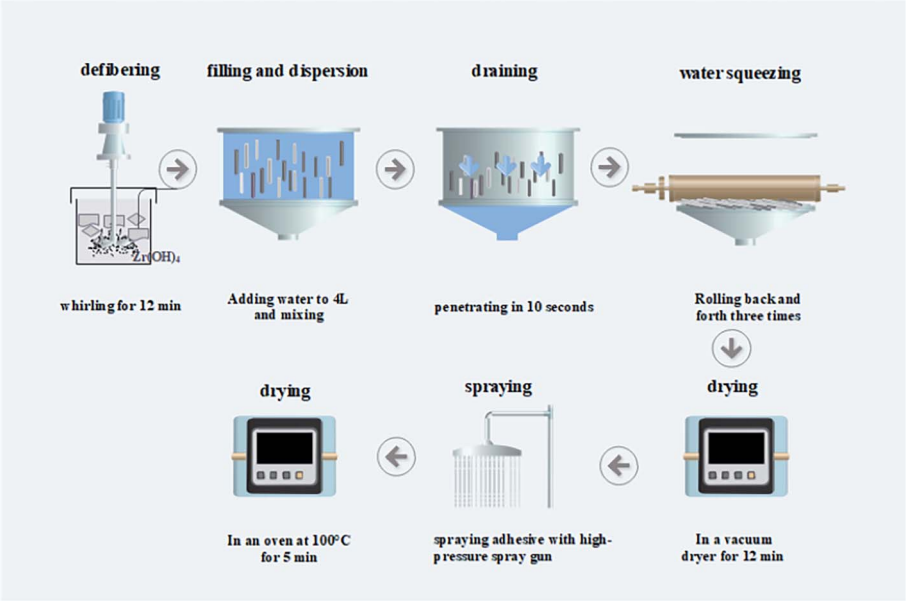

Fig. 1 Specific flow chart of SD-AFP preparation.

trifluoroacetamide (BSTFA) and 1% trimethylchlorosilane (TMCS), were used without any pre-treatment. Zirconium hydroxide (ZH, AR grade) was purchased from Shanghai Yingcheng New Material Co., Ltd. Acrylic resin emulsion (solid content 47%) was obtained from Shenzhen Jitian Chemical Co., Ltd. The blue reagent (T-135 reagent) was made in the laboratory by dissolving thymol phthalein (2.0 g) and potassium hydroxide (KOH, 0.6 g, AR grade) in 340 mL of anhydrous ethanol, and diluted to 400 mL with H_2O. HD and VX (of more than 98% purity) were supplied by synthetic chemistry division of our establishment. Due to their high toxicity and dangerousness, they were handled only by well-trained personnel using appropriate procedures carefully in very small quantities.

2.2 Preparation of SD-AFP

Wet papermaking, a widely used method for industrial paper production, mainly includes processes such as fiber decomposing, filling and dispersing, water pumping, water extrusion, and drying. Adding ZH to the pulp, the SD-AFP was prepared by this method. The specific flow chart is shown in Fig. 1.

An alkali-free glass fiber with a diameter of 3.0–4.0 μm and a diameter of 0.1–0.3 μm was used for paper-making. The moisture in the pulp was monitored using a HE53/02 Moisture Analyzer (Mettler-Toledo Instruments Co., Ltd, China). The pulp was weighed quantitatively according to the fiber grammage (50, 60, 70, 80 and 90 g m^{-2}), which refers to the weight of paper per square meter. The mass of requisite pulp was calculated using formula (1). The ZH powder was weighed according to the required retention rate (40, 80, 120, 150, and 180 wt%) and stirred with water.

$$m_1(\%) = \frac{g \times A}{100 - \theta} \times 100 \quad (1)$$

where m_1 is the mass of the pulp, g; g is the grammage of the SD-AFP, g m^{-2}; A is the area of papermaking, m^2; and θ is the moisture content of the pulp, %.

The weighed pulp was diluted with water to 2.5 L and defibered using a standard pulp disintegrator (TFO-KT, Hitachi, Japan) for 12 min. In order to promote fiber dispersion, dilute hydrochloric acid was added during the disintegration process, and the pH value was adjusted to 2.8–3.0. The ZH suspension was poured into the pulp and they were mixed thoroughly. The mixture was transferred into a 10 L cylinder, with a diameter of 200 mm, of a standard paper sheet former (P95854, PTI Ltd, Austria) to stir, filter and shape. Covered with a PTFE film and 10 layers of filter paper, the wet paper sheet was rolled back and forth 3 times with a roller to squeeze the residual moisture in the filter paper and immobilize the fibers. Then, the wet hand sheet was removed together with the PTFE film from the screen and they were placed in a vacuum dryer to dry for 12 min to obtain SD-AFP. The water-soluble acrylic resin emulsion was configured to different concentrations (1%, 2%, 4%, and 6%) and sprayed on the paper. Finally, it was placed in an oven at 100 °C for 5 min to dry. The formula of the retention rate is as follows:

$$L(\%) = \frac{m_3 - m_2}{m_2} \times 100 \quad (2)$$

where L is the retention rate of ZH, %; m_2 is the mass of the AFP without ZH, g; and m_3 is the mass of the SD-AFP, g.

2.3 Characterization

A field-emission scanning electron microscope (FE-SEM, Regulus 8100, Hitachi, Japan) equipped with an energy-dispersive spectrometer (EDX, XFlash-Detector 5010, Bruker) was used to observe the morphological changes of the AFP. Before the test, the samples were sprayed with gold using

Fig. 2 Optical images (a) SD-AFP. (b) Top view of the self-made container with SD-AFP. (c) Ichnography of the self-made container with SD-AFP.

a Sputter Coater 108 (Cressington, Oxhey, British). X-ray diffraction patterns of all samples were recorded using a Bruker D8 discover X-ray diffractometer (XRD) with Cu Kα radiation (operating at 40 kV and 30 mA). The 2θ scan was from 10° to 70° and the scanning speed was 8° min^{-1}. The samples were compactly placed on glass slides, which were positioned on the sample platform for analysis. Thermogravimetric analysis (TGA) measurement was obtained using a synchronous thermal analyzer (STA449F5, Netzsch, Germany). The samples were placed in a desiccator for pretreatment at ambient temperature for 24 h before analysis. The AFP was cut into tiny pieces of paper before being put into the sample tank. The samples, about 10 mg, were heated from 30 °C up to 800 °C. The heating rate was 10 °C min^{-1} and the total N_2 flow rate was 50 mL min^{-1}. The data were analyzed using the Netzsch Proteus Thermal Analysis software.

2.4 General performance test of SD-AFP

The test of tensile strength was conducted using an electronic universal material testing machine (3367, Instron, USA). Samples were cut into 250 mm × 10 mm and the tensile speed was set at 4 mm min^{-1}. The tensile strength can be calculated using formula.[3] The filtration efficiency was tested by an oil mist method. The oil mist generated by the spray generator was passed through the AFP, and the concentrations before and after the permeation were measured using a N840020 turbidimeter. The concentration of the oil mist with a particle size of 0.28–0.34 μm is 2000–2500 mg m^{-3} and the airflow velocity is 6.3 L min^{-1}. The pressure drop without AFP in the fixture is 137.2 Pa. The permeability coefficient (K_f, %) was calculated using formula (4) and the filtration efficiency (η, %) was calculated using formula (5). The pressure drop of the AFP was measured using an inclined micromanometer. The air viscosity

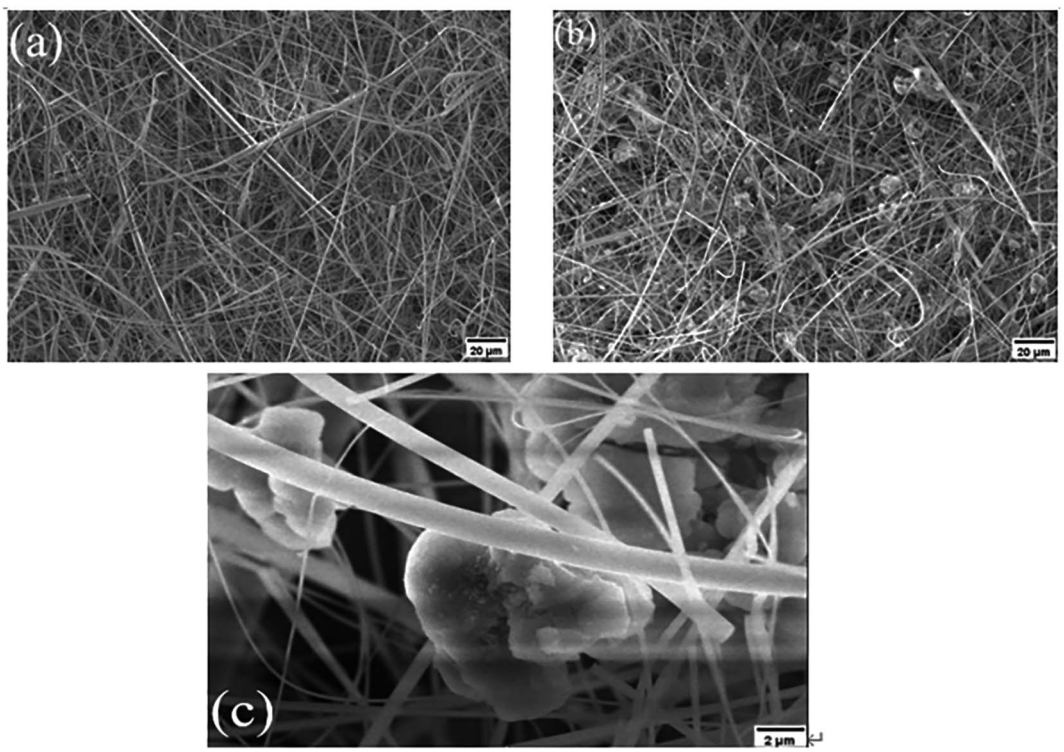

Fig. 3 FE-SEM images of AFP: (a) AFP without ZH × 500. (b) SD-AFP × 500. (c) SD-AFP × 5000.

is 17.9 × 10^{-6} Pa s^{-1} and the airflow velocity is identically 6.3 L min^{-1}.

$$S = \frac{F}{L_W} \tag{3}$$

$$K_f(\%) = \frac{C_t}{C_0} \times 100 \tag{4}$$

$$\eta = 1 - K_f \tag{5}$$

where S is the tensile strength, kN m^{-1}; F is the maximum load, N; L_W is the width of the test paper, mm; K_f is the transmittance of AFP, %; C_0 and C_t are the concentrations of oil mist before and after capturing respectively, mg m^{-3}; and η is the filtration efficiency of AFP, %.

2.5 Degradation performance test of the SD-AFP

2.5.1 Degradation of HD on the SD-AFP. Alkalized thymol phthalein (T-135 reagent), reacting with HD to become a stable orange–yellow substance after acidification, was used as an indicator to measure the concentration of HD. The absorbance was measured using an ultraviolet-visible spectrophotometer (λ_{max} = 447 nm, 722G, Electronic Analysis Instrument Co., Ltd, China). The calibration curve was obtained by plotting the assayed quantity (y-axis) *versus* the concentration (x-axis) of the HD solution. The concentration of HD (y, μg mL^{-1}) *versus* absorbance (x, Abs.) showed a good linear relationship and a linear regression equation C_{HD} = 151.55A was obtained with a linear correlation coefficient R^2 = 0.9994. First, 5 μL of HD was transferred as extremely tiny droplets on the well-prepared SD-AFP, positioned in the self-made container with grinding bottleneck (Fig. 2). Sealing with parafilm, the container was placed in a thermostat with a temperature of 25 ± 1 °C for different time periods. Then, 15 mL of petroleum ether, as extractant, was added into the container and shaken continuously for 20 s. After 15 min of sample resting, the petroleum ether phase was sampled for residual HD determination and the recovery calculation by the T-135 method.[3] Ultimately, the sample was diluted to 10 mL and shaken sufficiently for the measurement of absorbance. According to the standard curve, the concentration of residual HD can be obtained. The formula of decontamination rate is as follows. The reaction kinetics curve was plotted as the conversion rate (y-axis) *versus* the reaction time (x-axis).

$$D(\%) = \left(1 - \frac{C \times V}{m_0}\right) \times 100 \tag{6}$$

where D is the conversion rate of HD, %; C is the detected concentration of residual HD, mg L^{-1}; V is the volume of HD solution, L; and m_0 is the initial mass of HD, mg.

2.5.2 Degradation of VX on the SD-AFP. Similarly, 3 μL of VX was transferred onto the well-prepared SD-AFP to react for the different time intervals. The analytical method is as follows. The reaction was terminated with 10 mL of 0.05 mol L^{-1} borax aqueous solution and the total sample was extracted with 50 mL of dichloromethane, followed by shaking for 20 s and standing for 10 min. The organic phase was taken in an Eppendorf (EP)

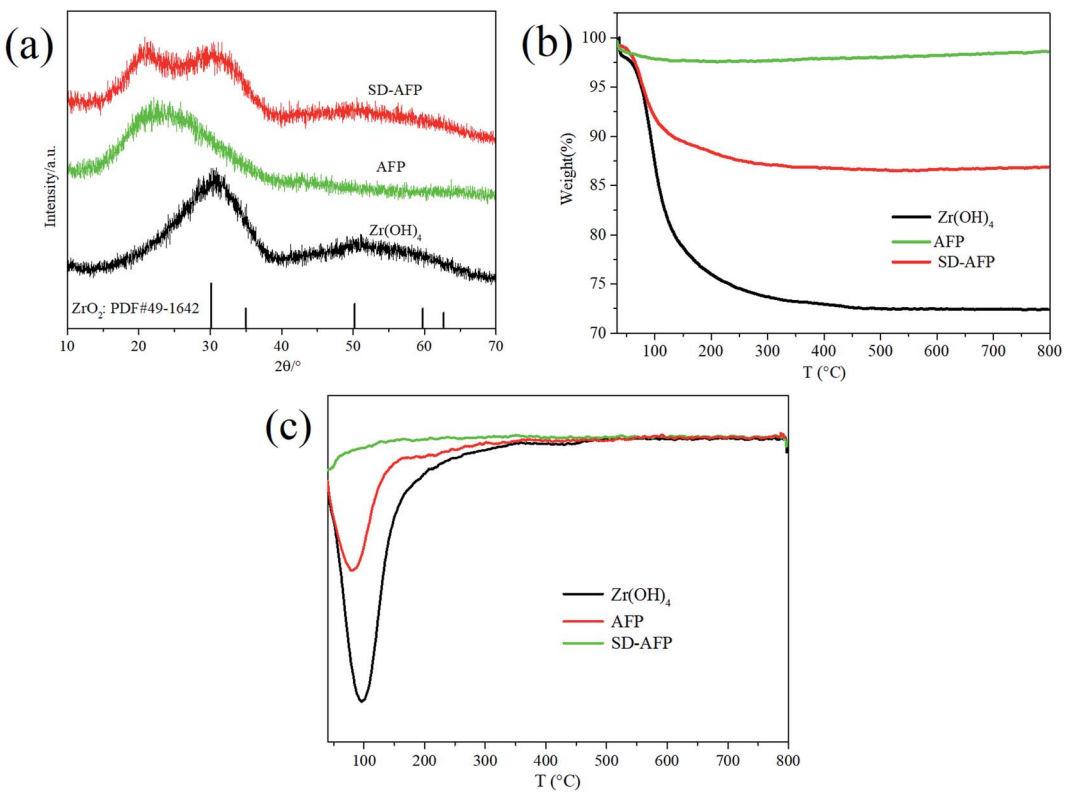

Fig. 4 Characterization of ZH powder and AFP. (a) XRD diagram. (b) TG diagram. (c) DTG diagram.

tube and anhydrous Na_2SO_4 was added for drying. Then, 2.5 mL of liquid was used for centrifugation using a TGL-16G Centrifuge (Anting Scientific Instrument Factory, China). The mixture of 1 mL of the centrifugal liquid and 30 μL of internal standard solution (40 mg tributyl phosphate and 10 mL CH_2Cl_2) was put in an EP tube for gas chromatography (GC, Agilent 6890N) equipped with a flame photometric detector (FPD). Qualitative and quantitative analyses depended on the retention time and internal standard method respectively. The conversion rate of VX was calculated using formula (7).

$$\Phi(\%) = \frac{A_{i0}/A_{s0}}{A_{ix}/A_{sx}} \times 100 \quad (7)$$

where Φ is the conversion rate of VX, %; A_{i0}/A_{s0} is the ratio of the chromatographic peak area of VX to the internal standard substance in the standard solution; and A_{ix}/A_{sx} is the ratio of the chromatographic peak area of VX to the internal standard substance in the degradation sample.

2.6 Detection of reaction products

Using acetonitrile instead of petroleum ether or CH_2Cl_2 as the extractant, reaction products were extracted directly and detected by gas chromatography-mass spectrometry using an Agilent Technologies instrument (7890A GC system coupled with 5975C MSD detector) equipped with an HP-5MS capillary column (30 m × 0.25 mm × 0.25 μm). The measurement conditions are as follows: carrier gas is high-purity helium at a flow rate of 50 mL min^{-1}, injection port temperature is 250 °C, detector temperature is 150 °C, ion source temperature is 230 °C, temperature programming is 50 °C for 1 minute, then 15 °C min^{-1} to 250 °C for 2 min. The shunt ratio is 20 : 1 and the ionization voltage is 70 eV.

Products with high polarity need to be derivatized before detection by GC-MS. The derivatization method is as follows. Reaction products were extracted with 5 mL of deionized water through ultrasonic shaking for 10 min, followed by centrifugation for 2 min at a speed of 7500 rpm. After transferring into a test tube, the aqueous solution was dried at 50 °C for 40 min using an RV8 rotary evaporator (IKA, Germany) at a speed of 200 rpm. Then, 100 μL of derivatization reagent was added and reacted in the water bath at 60 °C for 30 min. After cooling, 1 μL of liquid was taken for analysis by GC-MS.

3. Results and discussion

3.1 Characterization

3.1.1 FE-SEM and EDX analysis. The morphology and chemical composition of the prepared AFPs were characterized using FE-SEM images and EDX spectra. Fig. 3(a) shows the image of AFP at 500 times magnification, and Fig. 3(b) and (c) show SD-AFP at different magnifications. It could be observed that the porous structure was formed by a glass fiber as the skeleton shown in Fig. 3(a). After adding ZH to the pulp for papermaking, granular solids appeared among the fibers of the AFP and the distribution was uniform, indicating that the ZH was well dispersed. Fiber self-assembly builds a three-dimensional network structure. Small ZH particles aggregated into 1–8 μm of large particles, which were wrapped in the internal network and filled uniformly in the interstices so as to load firmly on the AFP. The EDX spectra of SD-AFP indicated not only that the composite material consists of C, O, Si, Na, Zr and other elements (Fig. S1†), but also that ZH was successfully loaded on the glass fiber of the AFP.

3.1.2 XRD analysis. There is a highly disordered structure in ZH, which can produce broad peaks in X-ray diffraction (XRD). The obtained XRD pattern (Fig. 4(a)) showed that there were two broad peaks at approximately 2θ = 20–40° and 2θ = 45–60°, which corresponded well to previous research results.[31–33] There were two sharper characteristic peaks near 2θ = 30.1° and 2θ = 50.2°, which closely corresponded to the (111) and (220) crystal planes of the standard spectrum of cubic zirconia (PDF#: 49-1642).[27] The width of these peaks indicated that they have an amorphous crystal structure with a short-range crystal order.[34] The XRD pattern of the AFP displayed that there was a broad peak at approximately 2θ = 15–35°. After adding ZH to the pulp for papermaking, the broad peaks of the two separate materials were previously superimposed, forming a hump and a broad peak at 15–40° and 45–60°, respectively. That is, the diffraction peaks of AFP and ZH were superposed simply, indicating that the crystal phases of the glass fiber and the ZH powder have not changed significantly and the ZH powder did not aggregate obviously during the in-pulp addition process.

3.1.3 TGA analysis. TGA analysis was performed on the prepared AFP without ZH, SD-AFP and original ZH powder. The TG and DTG diagram of materials are shown in Fig. 4(b) and (c), which corresponded well to previous studies.[35,36] The weight loss of the AFP without ZH during the whole heating process was only 1.4%, indicating that the alkali-free glass fiber was resistant to high temperatures, and the weight loss was mainly due to the adsorbed water molecules. In a wide temperature range of 30–200 °C, there was distinct weight loss on the SD-AFP and the ZH powder, which is mainly attributed to the evaporation of adsorbed water on the surface of the material and the removal of stronger binding force of water molecules in the pores.[37] It can also be observed from the analysis of the DTG curve that, unlike the AFP without ZH added, the SD-AFP and ZH powders both show a clear cliff-like decline, ending at

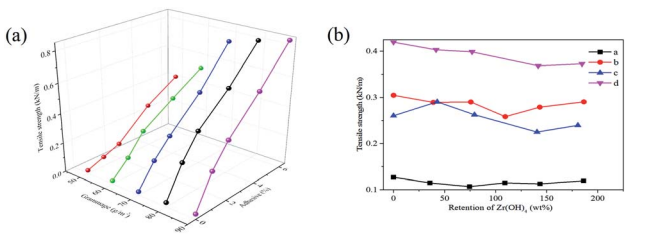

Fig. 5 Tensile strength of SD-AFP: (a) Three-dimensional graph of the tensile strength varies with the fiber grammage and the amount of adhesive (90 wt% ZH). (b) Tensile strength varies with the retention rate of ZH a. Grammage 50 g m^{-2}, adhesive 2%; b. Grammage 50 g m^{-2}, adhesive 4%; c. Grammage 60 g m^{-2}, adhesive 4%; d. Grammage 60 g m^{-2}, adhesive 4%.

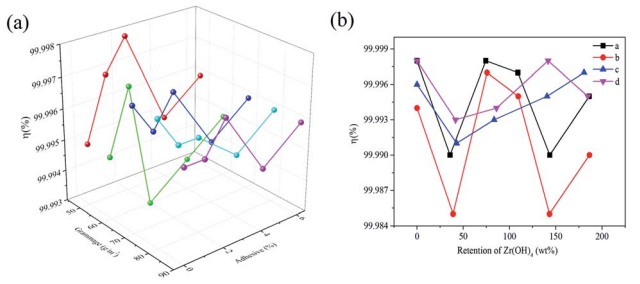

Fig. 6 Filtration efficiency of SD-AFP: (a) Three-dimensional graph of the filtration efficiency varies with the fiber grammage and the amount of adhesive (90 wt% ZH). (b) Filtration efficiency varies with the retention rate of ZH (a) grammage 50 g m^{-2}, adhesive 2%; (b) grammage 50 g m^{-2}, adhesive 4%; (c) grammage 60 g m^{-2}, adhesive 4%; (d) grammage 60 g m^{-2}, adhesive 4%.

350 °C. This process corresponds to the evaporation of adsorbed water and the decomposition of water of crystallization. The degree of weight loss of the two materials was gradual from 200 °C to 350 °C in the TG curve due to the change of the b-OH and t-OH groups forming oxide bonds during the crystallization into zirconium dioxide.[27,35] The final weight loss at 800 °C was 13.1% and 27.6%, respectively. The weight loss of SD-AFP was calculated as 28.4% converted by the retention rate of ZH, which is similar to the weight loss of powder. It was supposed that the structure of ZH did not significantly change and the weight loss was mainly attributed to the removal of adsorbed water and dihydroxylation.

3.2 Tensile strength

Fig. 5 shows that the tensile strength data of SD-AFP with different fiber grammage values, different addition amounts of adhesives and different retention rates of ZH were tested. As shown in Fig. S2(a),† as the grammage of the fiber increases, the tensile strength of the paper with different adhesives demonstrates a linear growth trend, and the relevant parameters of the fitted linear equation are shown in Table S1.† The bigger the fiber grammage, the more numerous the number of bonds between the fibers during the consolidation and drying processes, and the faster the increase in tensile strength. As the addition amount of adhesives increases, the tensile strength also shows a linear growth trend, as shown in Fig. S2(b).† The fitted linear relationship was good, whose R^2 was greater than 0.975, and the relevant parameters of the fitted linear equation are shown in Table S2.† When there was no adhesive added, the strength of the AFP was only 0.0221–0.0368 kN m^{-1}, and the paper was soft and easily broken. The more the adhesive was added, the stronger the fiber network would be combined, and

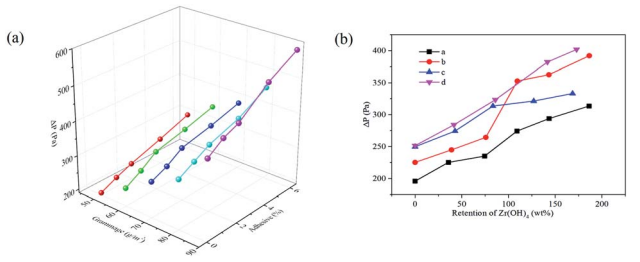

Fig. 7 Pressure drop of SD-AFP: (a) three-dimensional graph of the pressure drop varies with the fiber grammage and the amount of adhesive (90 wt% ZH). (b) Pressure drop varies with the retention rate of ZH. (a) grammage 50 g m^{-2}, adhesive 2%; (b) grammage 50 g m^{-2}, adhesive 4%; (c) grammage 60 g m^{-2}, adhesive 4%; (d) grammage 60 g m^{-2}, adhesive 4%.

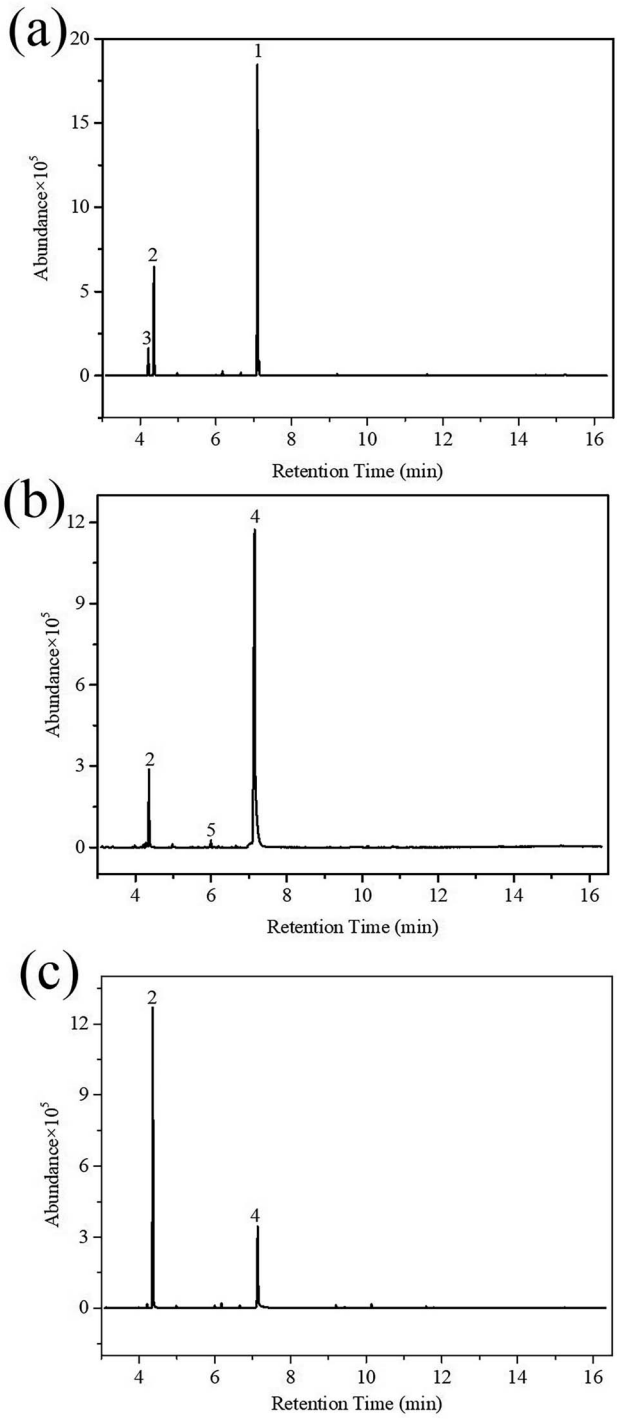

Fig. 8 GC/MS total ion chromatograms of HD reacted on SD-AFP for different time periods: (a) 5 h; (b) 24 h; and (c) 36 h.

Table 1 Possible degradation products of HD on SD-AFP detected by GC/MS[a]

No.	t_R/min	Structural formula	Fragment peak (m/z)
2	4.360	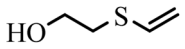	45, 61, 73, 91, 109, 140
3	4.215	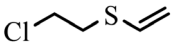	45, 60, 73, 122
4	7.133	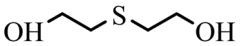	61, 75, 91, 104, 122
5	5.996	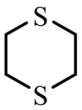	61, 64, 66, 73, 87, 92, 105, 120

[a] 1# is undecomposed mustard gas, which is not presented in the table.

the faster the tensile strength would increase. When 2% and 4% adhesives were added, the strength was 0.1658–0.3984 kN m^{-1} and 0.2902–0.6099 kN m^{-1}, respectively. The paper with 6% adhesives was brittle and easy to break. From the comparison of the linear slopes, the change in tensile strength caused by the addition of adhesives was larger, displaying that it was a pivotal factor in determining the tensile strength.

When the grammage was 50 g m^{-2} and 60 g m^{-2}, the increase in tensile strength was smaller than when the grammage was larger. As shown in Fig. 5(b), as the retention rate of ZH increases, the tensile strength fluctuates up and down in a broken line. However, the standard deviation was less than 0.0250 kN m^{-1} and the RSD was less than 10%. In particular, when the grammage was 60 g m^{-2} and the addition of adhesive was 4%, the strength showed a downward trend. Although ZH would play a supporting role between the fibers, the agglomerated ZH destroyed more severely the stacking structure between the original fibers, making them not tightly bonded. As a result, the tensile strength descended slightly as the ZH increased.

3.3 Filtration efficiency

Fig. 6 displays that the filtration efficiency data of SD-AFP with different fiber grammage values, different addition amounts of adhesives and different retention rates of ZH were tested. When the grammage of the fiber was 50–90 g m^{-2} and the addition amount of adhesives was 0–6%, the filtration efficiency showed different degrees of oscillation trend. The fluctuation range was between 99.993–99.998%, and all of them were greater than 99.990%, which reached the filtration requirement of high-efficiency AFP. The chopped glass fiber with a relatively thick diameter acts as a structural substance in the paper sheet to form a three-dimensional framework structure, while the finer glass wool is randomly distributed and entangled on the framework. The combination of thick and thin fibers creates a structure with small pores and large porosity, which has excellent filtering performance.[38,39]

The filtration efficiency varies with the retention rate of ZH, as shown in Fig. 6(b). It can be observed that the filtration efficiency of AFP without ZH was 99.994–99.998%. When ZH was added to the pulp for papermaking, it was reduced by 0.009% and increased by 0.002% at most, and the standard deviation was less than 0.006%. It may be due to the influence of ZH on the fiber bonding state and changes in the pore diameter.

3.4 Pressure drop

Fig. 7 demonstrates that the pressure drop data of SD-AFP with different fiber grammage values, different addition amounts of adhesives and different retention rates of ZH were tested. As the amounts of adhesives increased, the pressure drop of different fiber grammage values showed a linear growth trend, as shown in Fig. S4(a),† and the relevant parameters of the fitted linear equation are shown in Table S3.† When the grammage was 80 g m^{-2} and 90 g m^{-2}, the linear slopes were bigger than 20, and the pressure drop increased rapidly with the increase in the amounts of adhesives. This may be due to the dense fiber network and the adhesive sprayed on the SD-AFP that blocked the originally few pores, resulting in difficulty in air flow and a steep increase in pressure drop. When the grammage was 50 g m^{-2} and 60 g m^{-2}, the pressure drop value was less than 350.0 Pa. As the grammage of the paper increased, the pressure drop of the paper with different adhesives increased linearly, as shown in Fig. S4(b),† and the relevant parameters of the fitted linear equation are shown in Table S4.† The bigger the fiber grammage, the greater the number of bonds between the fiber

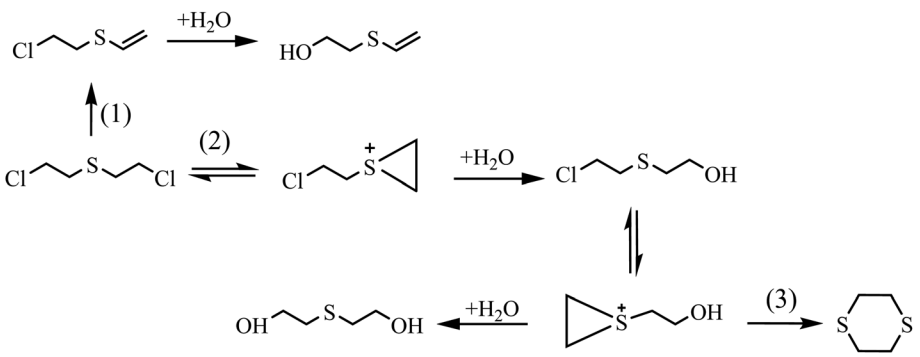

Fig. 9 Reaction pathways of HD on SD-AFP.

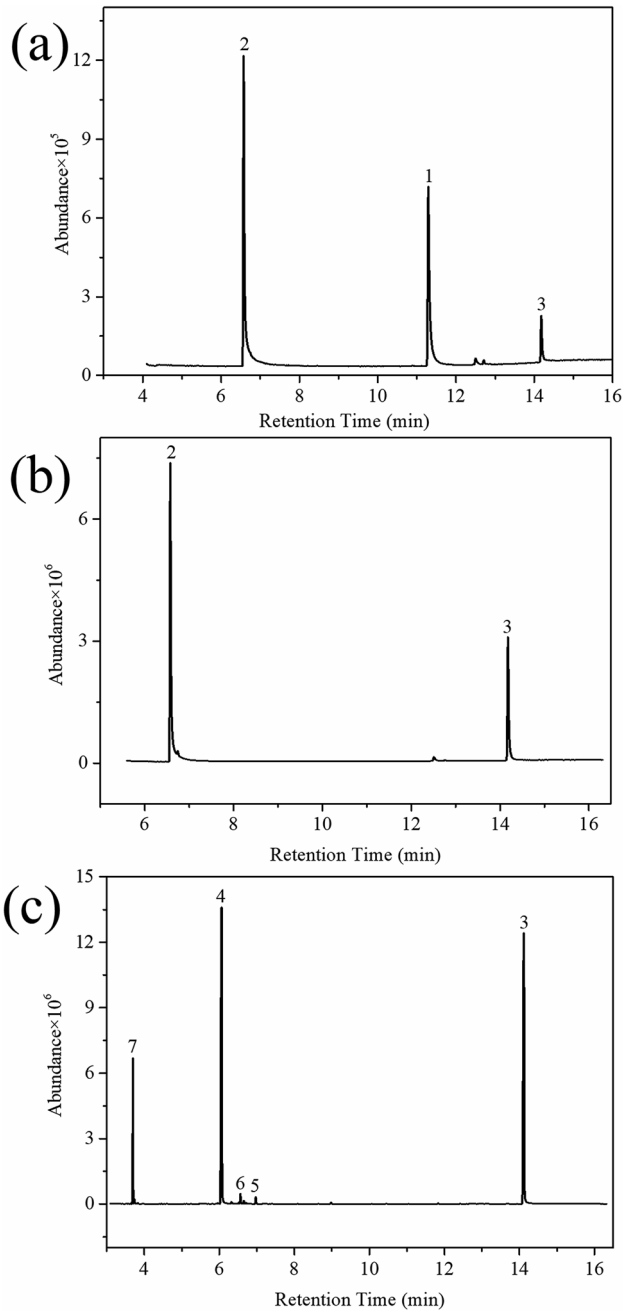

Fig. 10 GC/MS total ion chromatograms of VX reacted on SD-AFP for different time periods: (a) 0.5 h; (b) 24 h; and (c) 24 h, derivatization-GC-MS spectrogram.

network during the consolidation and drying processes, and the longer the airflow passes, resulting in the greater pressure drop.

As presented in Fig. 7(b) and Table S5,† as the retention rate of ZH increased, the pressure drop occurred with linear growth, which may be due to the addition of ZH causing the average pore diameter to become smaller. When the fiber grammage was 50 g m^{-2} and 60 g m^{-2}, the pressure drop of paper with 4% adhesive was 1.54 and 1.77 times of 2% adhesive, respectively, indicating that the three factors all have a positive correlation effect on pressure drop.

Considering the three indicators of tensile strength, filtration efficiency and pressure drop comprehensively, the SD-AFP with the grammage of 50 g m^{-2} and the adhesive of 2% was selected for the further study of the decontamination of HD and VX.

3.5 Reaction products and mechanism

3.5.1 Reaction products and mechanism of HD. GC/MS was used to detect the degradation products of HD on the SD-AFP, and the total ion chromatograms of HD reacted on SD-AFP for 5 h, 24 h, and 36 h, as shown in Fig. 8. According to the retention time of the chromatographic peak and MS fragment peak, the structure formulas of possible degradation products were inferred in Table 1. Combining the analysis of Fig. 8 and Table 1, the specific reaction pathway is displayed in Fig. 9.

HD did not degrade completely at 5 h, and the products 2-hydroxyethyl vinyl sulfide (2#) and 2-chloroethyl vinyl sulfide (3#) were obtained. After 24 h, HD was not present and 3# disappeared, indicating that 3# was an intermediate product. The reaction pathway (1) can be speculated as follows, and the α-C of HD was attacked by an alkaline terminal hydroxyl group of ZH, causing the elimination of H on it to obtain a vinyl group. In addition, the nucleophilic substitution reaction resulting from the attack of the hydroxide ion on the C^+ ion in the C–Cl bond occurred. Meanwhile, thiodiglycol (4#), a predominant degradation product that still exists in the last spectrogram, was generated through basic hydrolysis as pathway (2).[40] 1,4-Dithiane (5#), just a tiny peak in Fig. 8(b), was a by-product, which may be obtained from the internal displacement of sulfonium ions during the hydrolysis process (pathway 3).[41]

3.5.2 Reaction products and mechanism of VX. The GC/MS total ion chromatograms of VX that reacted on SD-AFP for 0.5 h and 24 h are shown in Fig. 10. According to the retention time of the chromatographic peak and the MS fragment peak, the structural formulas of the possible degradation products were inferred in Table 2. Non-polar or weakly polar products of VX were detected by GC-MS directly. As shown in Fig. 10(a) and (b), VX still existed at 0.5 h and degraded completely after 24 h reaction. The main products including 2-(diisopropylamino)-ethanethiol (2#) and disulfide (3#) were detected. Nevertheless, the other half of the decomposition was not found in the spectrogram. Some of the hydrolysates of the nerve agent are a kind of highly polar compounds that are easily soluble in water and hardly volatile, which must be derivatized before GC analysis.[42–44] The pre-column derivatization-GC-MS method was used to detect the polar products of VX. As presented in Fig. 10(c), the dominating products were disulfide (3#) and silanized methyl ethyl phosphate (EMPA, 4#), ethoxymethyl thiophosphonic acid (EMPTA, 5#) and 2-diisopropylamine ethanol (6#). The phosphate product was consistent with the product obtained by nuclear magnetic resonance (NMR).[24]

Combining the analysis of Fig. 10 and Table 2, the specific reaction pathway of VX on the SD-AFP was shown in Fig. 11. It may undergo three degradation pathways: (1) the primary reaction is a nucleophilic substitution reaction caused by the attack of hydroxide ions on P^+ in the P–S bond; (2) the H atom

Table 2 Possible degradation products of VX on SD-AFP detected by GC/MS[a]

No.	t_R/min	Structural formula	Fragment peak (m/z)
2	6.579	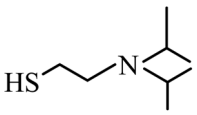	58, 72, 86, 114, 128, 146, 161
3	14.114	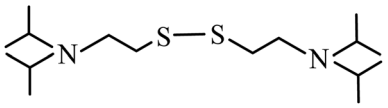	56, 72, 84, 98, 114, 128, 144, 160, 193
4	6.060	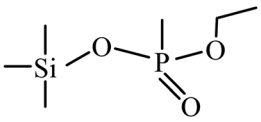	61, 75, 91, 121, 137, 153, 169, 181, 196
5	6.560	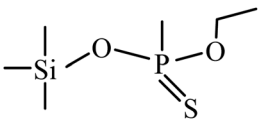	59, 75, 91, 103, 121, 137, 153, 169, 197, 209
6	6.969	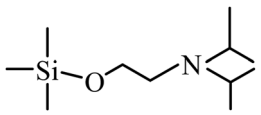	59, 72, 84, 100, 114, 144, 160, 202, 217

[a] 1# is undecomposed VX and 7# is the derivatization reagent, which are not presented in the table.

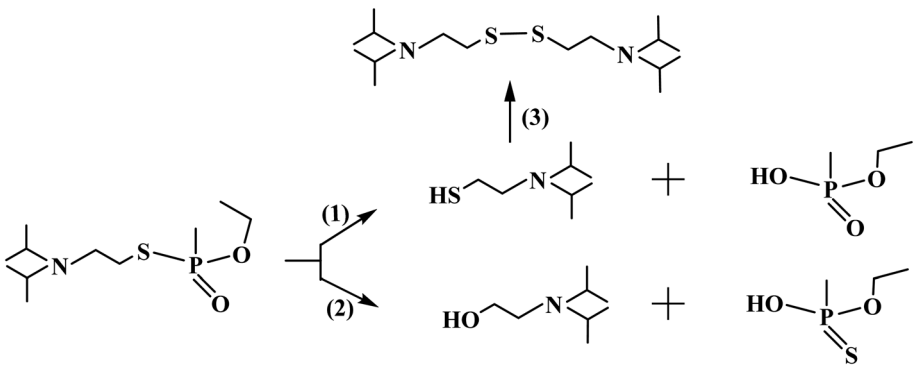

Fig. 11 Reaction pathways of VX on SD-AFP.

on α-C connected to the S atom on VX is acidic and reacts with the basic group of ZH, resulting in the cleavage of S–C;[45] and (3) polymerization of sulfur-containing compounds.

The reaction products were non-toxic or low-toxic, indicating that SD-AFP has a good degradation effect on HD and VX. In order to lucubrate its effect in depth, the kinetics of the reaction was investigated.

3.6 Degradation of HD and VX on SD-AFP

Fig. 12(a) exhibits the variation curve of the conversion rate of HD and VX on the SD-AFP for 24 h, which varies with the retention rate of ZH. When the density of HD on the SD-AFP was 5.0 g m^{-2}, the conversion rate increased slowly at first and then quickly, which was 92.0% at a retention rate of 183.0 wt%. When the density of HD was reduced to 2.2 g m^{-2}, the retention rate of ZH reaching 125.0 wt% could completely degrade HD (conversion rate >99.0%). When the density of VX was 1.1 g m^{-2}, the conversion rate was 84.9% at a retention rate of 42.6 wt%, and the retention rate reaching 175.0 wt% could completely degrade VX. SD-AFP, which can completely decompose both HD and VX within 24 h, had a tensile strength of 0.1193 kN m^{-1}, a filtration efficiency of 99.995%, and a pressure drop of 313.6 Pa.

The degradation of HD and VX on ZH powder and SD-AFP was compared, as shown in Fig. 12(b) and (c). HD and VX were reacted on SD-AFP with the retention rate of (125 ± 5) wt% and (175 ± 5) wt% that can be thoroughly decomposed in 24 h, respectively. Taking the reaction time in the x-axis and the

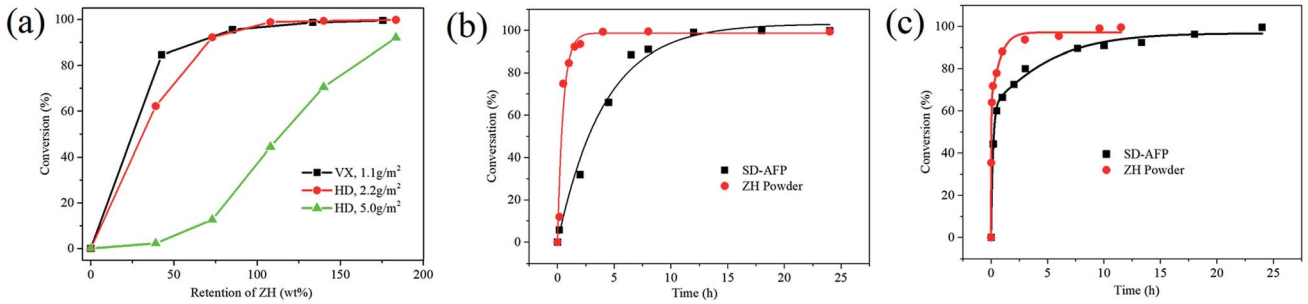

Fig. 12 Degradation of HD and VX on SD-AFP: (a) conversion rate varies with the retention rate of ZH (24 h); (b) conversion rate of HD varies with the reaction time; and (c) conversion rate of VX varies with the reaction time.

disinfection rate in the y-axis, the relationship between the conversion rate and the reaction time was obtained.

The degradation rate of HD presented a faster trend first and then a slower trend, which conformed to the pseudo-first-order reaction kinetics (eqn (8)). The reaction rate constant (k_1) was derived from the slope of linear plots $\ln(C_0/C_t)$ *versus* t and the half-life ($t_{1/2}$) was calculated from $\ln(2)/k_1$, which are shown in Table 3. The conversion rate of VX rose rapidly and then tended to be flat over time. Compared with HD, the decomposition of VX was faster at the beginning. On the one hand, the reaction processes of ZH powder with HD and VX were different and the half-lives were 30.6 min and 1.8 min, respectively. On the other hand, VX spread faster on SD-AFP as its surface tension is less than that of HD. However, VX is large in size and slow in transportation, so the late reaction rate was slower. The simple first-order reaction kinetics cannot fully conform to the reaction process, so the logistic function[46] was introduced, which emphasized the importance of the dispersion of VX. Eqn (9) accorded with the conversion rate of VX *vs.* reaction time and R^2 were all greater than 0.99 (Table 4).

$$\ln(C_0/C_t) = k_1 t \tag{8}$$

$$y = \frac{1 - e^{-k_1 t}}{1 + e^{k_0 - k_2 t}} \tag{9}$$

where C_0 is the initial concentration of HD, mg L^{-1}; C_t is the detected concentration of residual HD, mg L^{-1}; t is the reaction time, h; k_1 is the reaction rate constant, h^{-1}; y is the conversion rate, %; k_0 is the kinetics constant, related to reaction conditions, h^{-1}; k_2 is the dispersion rate constant, h^{-1}.

The reaction between ZH and poison droplets is a liquid–solid reaction. It is more difficult to carry out than the homogeneous reaction in theory, but k_1 were 1.4 h^{-1} and 44.6 h^{-1} respectively, indicating that ZH had a good degradation effect on HD and VX. Compared with the ZH powder, the time for HD and VX to reach reaction equilibrium on the SD-AFP was longer, and the $t_{1/2}$ value obtained by fitting was 2.1 h and 0.27 h longer, respectively. The ZH powder was shaken and it was more conducive to the contact between the poison and the decontaminant, so as to carry out the reaction. The ZH added in the pulp was mostly distributed in the fiber network, and poison needed to diffuse and penetrate to reach the decontaminant inside the paper. Therefore, k_1 of poison droplets on the SD-AFP was much smaller than the k_1 value of it on the ZH powder. From the perspective of k_2, the diffusion process of VX on SD-AFP was 1.0 h^{-1} smaller than that of the powder, manifesting that the dispersion and penetration of poison droplets on SD-AFP were tardy, and the contact with the decontaminant was insufficient. As a result, it was of more difficulty to proceed from the view of mass transfer.

Table 3 Decontamination kinetic parameters of HD

Decontaminant	k_1/h^{-1}	$t_{1/2}$/h	R^2
ZH powder	1.4	0.5	0.9742
SD-AFP	0.3	2.6	0.9920

Table 4 Decontamination kinetic parameters of VX

Decontaminant	k_1/h^{-1}	k_0/h^{-1}	k_2/h^{-1}	$t_{1/2}$/h	R^2
ZH powder	44.6	−0.7	1.2	3.0×10^{-2}	0.9922
SD-AFP	5.4	−0.6	0.2	0.3	0.9940

4. Conclusions

In this work, a self-decontaminating air filter paper that can simultaneously degrade HD and VX has been successfully prepared using zirconium hydroxide as a decontaminant and an intra-pulp addition technology. Based on FE-SEM, EDX, XRD and TGA analysis, it was found that ZH was uniformly distributed and attached in the interstices of the glass fiber. Compared to the base paper and ZH powder, the glass fiber and ZH used for the composite material had no obvious crystalline changes, and ZH had no distinct aggregation. Taking filtration efficiency, pressure drop and tensile strength as evaluation indicators, the influence of the fiber grammage, amount of adhesive and retention of ZH on the general performance of SD-AFP was investigated. The SD-AFP with a fiber grammage of 50 g m^{-2} and the addition of adhesive of 2% had high filtration efficiency, low breathing pressure drop and moderate tensile strength, which was used to conduct degrading experiment. It

was discovered that HD and VX were both converted into non-toxic or low-toxic products through the degradation effect research. The half-lives of HD and VX on SD-AFP were 2.6 h and 16.2 min, respectively. It is displayed that the in-pulp addition technology of preparing SD-AFP is feasible, which have achieved the aim to degrade HD and VX. Further research will be devoted to the exploitation of new technology and the optimization of technological conditions to decrease the pressure drop.

Author contributions

X. Q. Huang: conceptualization, data curation, formal analysis, investigation, writing original draft. T. Zhao: funding acquisition, resources, investigation, project administration. H. P. Zhang: data curation, methodology, writing–review and editing. C. X. Yan: funding acquisition, formal analysis, writing–review and editing. J. L. Sha: formal analysis, resources. H. M. Tang: investigation. H. Y. Zhu: resources. W. Yue: investigation.

Conflicts of interest

The authors declare no competing financial interest.

Acknowledgements

This work is supported by the National Defence Preresearch Foundation of China (30110020302).

References

1 T. T. Marrs, R. L. Maynard and F. R. Sidell, *Chemical Warfare Agents, Toxicology and Treatment*, John Wiley & Sons Ltd, England, 1966, pp. 1–230.
2 W. H. Gary and R. S. Erik, Persistent effects of chlorine inhalation on respiratory health, *Ann. N. Y. Acad. Sci.*, 2016, **1378**, 33–40.
3 E. Lopez-Maya, C. Montoro, L. M. Rodriguez-Albelo, S. D. Aznar Cervantes, A. A. Lozano-Perez, J. L. Cenis, E. Barea and J. A. Navarro, Textile/metal–organic-framework composites as self-detoxifying filters for chemical-warfare agents, *Angew. Chem., Int. Ed.*, 2015, **54**, 6790–6794.
4 Y. Q. Li, Q. Gao, Y. S. Zhou, L. J. Zhang, Y. X. Zhong, Y. Ying, M. C. Zhang and Y. A. Wang, Significant enhancement in hydrolytic degradation of sulfur mustard promoted by silver nanoparticles in the Ag NPs@HKUST-1 composites, *J. Hazard. Mater.*, 2018, **358**, 113–121.
5 X. Zhang, Y. Li, S. Wang and X. Wang, Polyoxometalate Immobilized on Graphene *via* Click Reaction for Simultaneous Dismutation of H_2O_2 and Oxidation of Sulfur Mustard Simulant, *ACS Appl. Nano Mater.*, 2019, **2**, 6971–6981.
6 L. Bromberg, W. R. Creasy, D. J. McGarvey, E. Wilusz and T. A. Hatton, Nucleophilic Polymers and Gels in Hydrolytic Degradation of Chemical Warfare Agents, *ACS Appl. Mater. Interfaces*, 2015, **7**, 22001–22011.
7 L. Bromberg, X. Su, V. Martis, Y. F. Zhang and T. A. Hatton, Self-Decontaminating Fibrous Materials Reactive toward Chemical Threats, *ACS Appl. Mater. Interfaces*, 2016, **8**, 17555–17564.
8 K. O. Kirlikovali, Z. J. Chen, T. Islamoglu, J. T. Hupp and O. K. Farha, Zirconium-Based Metal–Organic Frameworks for the Catalytic Hydrolysis of Organophosphorus Nerve Agents, *ACS Appl. Mater. Interfaces*, 2020, **12**, 14702–14720.
9 W. John, S. G. Heidi and Y. Walter, *Effect of Membrane Structure upon the Reactivity of CWA Deactivating Compounds-Implications for Self-Decontaminating Textiles*, 7th CBW Protection Symposium, Stockholm, Sweden, 2001.
10 T. Islamoglu, Z. J. Chen, M. C. Wasson, C. T. Buru, K. O. Kirlikovali, U. Afrin, M. R. Mian and O. K. Farha, Metal–Organic Frameworks against Toxic Chemicals, *Chem. Rev.*, 2020, **120**, 8130–8160.
11 M. Kalaj, K. C. Bentz, S. A. Jr, J. M. Palomba, K. S. Barcus, Y. Katayama and S. M. Cohen, MOF-Polymer Hybrid Materials: From Simple Composites to Tailored Architectures, *Chem. Rev.*, 2020, **120**, 8267–8302.
12 A. Phadatare and B. Kandasubramanian, Metal Organic Framework Functionalized Fabrics for Detoxification of Chemical Warfare Agents, *Ind. Eng. Chem. Res.*, 2019, **59**, 569–586.
13 M. J. Geraci, Mustard gas: imminent danger or eminent threat?, *Ann. Pharmacother.*, 2008, **42**, 237–246.
14 K. Ghabili, P. S. Agutter, M. Ghanei, K. Ansarin, Y. Panahi and M. M. Shoja, Sulfur mustard toxicity: history, chemistry, pharmacokinetics, and pharmacodynamics, *Crit. Rev. Toxicol.*, 2011, **41**, 384–403.
15 A. Richardt and M. Blum, *Decontamination of Warefare Agents*, Wiley Online Books, 2008, pp. 57–59.
16 R. Harris and J. Paxman, *A Higher Form of Killing*, Hill and Wang, New York, 1982, p. 53.
17 G. Mogilevsky, C. J. Karwacki, G. W. Peterson and G. W. Wagner, Surface hydroxyl concentration on $Zr(OH)_4$ quantified by 1H MAS NMR, *Chem. Phys. Lett.*, 2011, **511**, 384–388.
18 J. Nawrocki, M. Rigney, A. Mccormicka and P. Carr, Chemistry of zirconia and its use in chromatography, *J. Chromatogr. A*, 1993, **657**, 229–282.
19 S. Sonal, P. Prakash, B. K. Mishra and G. C. Nayak, Synthesis, characterization and sorption studies of a zirconium(IV) impregnated highly functionalized mesoporous activated carbons, *RSC Adv.*, 2020, **10**, 13783–13798.
20 S. Sonal and B. K. Mishra, A comprehensive review on the synthesis and performance of different zirconium-based adsorbents for the removal of various water contaminants, *Chem. Eng. J.*, 2021, **424**, 130509.
21 L. H. Velazquez-Jimenez, R. H. Hurt, J. Matos and J. R. Rangel-Mendez, Zirconium–carbon hybrid sorbent for removal of fluoride from water: oxalic acid mediated Zr(IV) assembly and adsorption mechanism, *Environ. Sci. Technol.*, 2014, **48**, 1166–1174.
22 G. Alagumuthu and M. Rajan, Equilibrium and kinetics of adsorption of fluoride onto zirconium impregnated cashew nutshell carbon, *Chem. Eng. J.*, 2010, **158**, 451–457.

23 J. Seokmin, S. Igor, P. Pehr and B. Robert, Kinetics of Dimethyl Methylphosphonate Adsorption and Decomposition on Zirconium Hydroxide Using Variable Temperature *in Situ* Attenuated Total Reflection Infrared Spectroscopy, *ACS Appl. Mater. Interfaces*, 2020, **12**, 14662–14671.

24 T. J. Bandosz, M. Laskoski, J. Mahle, G. Mogilevsky, G. W. Peterson, J. A. Rossin and G. W. Wagner, Reactions of VX, GD, and HD with $Zr(OH)_4$: Near Instantaneous Decontamination of VX, *J. Phys. Chem. C*, 2012, **116**, 11606–11614.

25 S. Jeon, R. B. Balow, G. C. Daniels, J. S. Ko and P. E. Pehrsson, Conformal Nanoscale Zirconium Hydroxide Films for Decomposing Chemical Warfare Agents, *ACS Appl. Nano Mater.*, 2019, **2**, 2295–2307.

26 Y. L. Liao, W. K. Chen, S. Z. Li, W. L. Jiao, Y. Si, J. Y. Yu and B. Ding, Ultrathin Zirconium Hydroxide Nanosheet-Assembled Nanofibrous Membranes for Rapid Degradation of Chemical Warfare Agents, *Small*, 2021, **17**, 2101639.

27 S. Kim, W. B. Ying, H. Jung, S. G. Ryu, B. Lee and K. J. Lee, Zirconium Hydroxide-coated Nanofiber Mats for Nerve Agent Decontamination, *Chem.–Asian J.*, 2017, **12**, 698–705.

28 Y. H. Ji, H. Qiao and Y. Liang, Preparation of Water-based Epoxy Resin and Its Application as an Automotive Air Filter Paper Binder, *Bioresources*, 2019, **14**, 7148–7156.

29 L. F. Hui, B. Yang, X. Han and M. R. Liu, Application of Synthetic Fiber in Air Filter Paper, *Bioresources*, 2018, **13**, 4264–4278.

30 J. Shen, Z. Song and X. Qian, A review on use of fillers in cellulosic paper for functional applications, *Ind. Eng. Chem. Res.*, 2010, **50**, 661–666.

31 P. D. Southon, J. R. Bartlett, J. L. Woolfrey and B. Ben-Nissan, Formation and Characterization of an Aqueous Zirconium Hydroxide Colloid, *Chem. Mater.*, 2002, **14**, 4313–4319.

32 Y. Kamimura and A. Endo, CO_2 adsorption–desorption performance of mesoporous zirconium hydroxide with robust water durability, *Phys. Chem. Chem. Phys.*, 2016, **18**, 2699–2709.

33 S. Jang, D. Ka, H. Jung, M. K. Kim, H. Jung and Y. Jin, $Zr(OH)_4$/GO Nanocomposite for the Degradation of Nerve Agent Soman (GD) in High-Humidity Environments, *Materials*, 2020, **13**, 2954.

34 B. B. Robert, G. Jeffrey, D. Lun, C. Grant, W. O. Daniels, M. M. Gordon, G. W. Peterson, J. H. Wynne and E. P. Pehr, Environmental Effects on Zirconium Hydroxide Nanoparticles and Chemical Warfare Agent Decomposition: Implications of Atmospheric Water and Carbon Dioxide, *ACS Appl. Mater. Interfaces*, 2017, **9**, 39747–39757.

35 G. W. Peterson and A. R. Joseph, Removal of Chlorine Gases from Streams of Air Using Reactive Zirconium Hydroxide Based Filtration Media, *Ind. Eng. Chem. Res.*, 2012, **51**, 2675–2681.

36 G. W. Peterson, J. A. Rossin, C. J. Karwacki and T. G. Glover, Surface chemistry and morphology of zirconia polymorphs and the influence on sulfur dioxide removal, *J. Phys. Chem. C*, 2011, **115**, 9644–9650.

37 D. Qin, E. Yan, J. Yu, W. Zhang, B. Liu and X. Yang, Synthesis of polymer/zirconium hydroxide core–shell microspheres and the hollow porous zirconium oxide microspheres, *Mater. Chem. Phys.*, 2012, **136**, 688–697.

38 Y. J. Yang, S. C. Zhang, X. L. Zhao, J. Y. Yu and B. Ding, Sandwich structured polyamide-6/polyacrylonitrile nanonets/bead-on-string composite membrane for effective air filtration, *Sep. Purif. Technol.*, 2015, **152**, 14–22.

39 X. L. Zhao, Y. Y. Li, T. Hua, P. Jiang, X. Yin, J. Y. Yu and B. Ding, Low-resistance Dual-purpose Air Filter Releasing Negative Ions and Effectively Capturing $PM_{2.5}$, *ACS Appl. Mater. Interfaces*, 2017, **9**, 12054–12063.

40 X. Q. Huang, T. Zhao, C. X. Yan, Y. R. Jin, Y. Wu and L. X. Zhang, Decontamination performance of air filter paper impregnated with zirconium hydroxide on sulfur mustard, *E3S Web Conf.*, 2021, **267**, 02063.

41 H. R. Tang, Z. X. Cheng, H. Y. Zhu, G. M. Zuo and M. Zhang, Effect of acid and base sites on the degradation of sulfur mustard over several typical oxides, *Appl. Catal., B*, 2008, **79**, 323–333.

42 Q. Q. Wang, J. W. Xie, M. S. Gu and J. X. Ruan, Chromatography and mass spectrometry in determination of nerve agents and their degradation products, *Milit. Med. Sci.*, 2005, **3**, 294–299.

43 V. Singh, S. Chinthakindi, A. K. Purohit, D. Pardasani, V. Tak and D. K. Dubey, Single vial sample preparation of markers of nerve agents by dispersive solid-phase extraction using magnetic strong anion exchange resins, *J. Chromatogr. A*, 2015, **1395**, 48–56.

44 R. Subramaniam, C. Astot, L. Juhlin, C. Nilsson and A. Ostin, Determination of *S*-2-(*N*,*N* diisopropylaminoethyl)- and *S*-2-(*N*,*N*-diethylaminoethyl) methylphosphonothiolate, nerve agent markers, in water samples using strong anion-exchange disk extraction, in vial trimethylsilylation, and gas chromatography-mass spectrometry analysis, *J. Chromatogr. A*, 2012, **1229**, 86–94.

45 M. B. Robin and M. Bob, Derivatisation reactions in the chromatographic analysis of chemical warfare agents and their degradation products, *J. Chromatogr. A*, 2003, **1000**, 253–281.

46 E. Couto, M. L. Calijuri, P. Assemany and P. R. Cecon, Evaluation of high rate ponds operational and design strategies for algal biomass production and domestic wastewater treatment, *Sci. Total Environ.*, 2021, **791**, 148362.